2013 European Control Conference (ECC)
July 17-19, 2013, Zürich, Switzerland.

Optimal Vehicle Dynamics Control for Combined Longitudinal and Lateral Autonomous Vehicle Guidance

Alexander Katriniok, Jan P. Maschuw, Fréderic Christen, Lutz Eckstein and Dirk Abel

Abstract— **This contribution proposes a model-based predictive control approach for combined longitudinal and lateral vehicle guidance. The controller, which has been designed for an automotive collision avoidance system, aims at following a desired evasion trajectory at the handling limits. Thereby, the trajectory following problem is decomposed in a path following and a velocity trajectory tracking problem using the wheel steering angle and the longitudinal acceleration as control inputs. There are two major advantages of this approach. First, the a priori knowledge of the evasion trajectory is explicitly incorporated into the computation of control inputs. Second, the combined transmission of longitudinal and lateral tire forces is considered in the sense of an integrated vehicle dynamics control approach. Experimental results show the potential of the introduced control scheme.**

I. INTRODUCTION

A. Motivation

Safety is one of the most important issues in the development process of a passenger vehicle. While passive safety systems like seat belts or air bags are already part of almost each vehicle, active safety systems resp. advanced driver assistance systems (ADAS) are increasingly employed in nowadays cars, see [1]. While antilock braking systems (ABS) or electronic stability controls (ESC) are applied to stabilize the ego-vehicle in critical driving situations, recent ADAS developments aim at taking the surrounding vehicle environment into account to avoid road accidents. Emergency brake assistant systems that conduct a partial or full braking maneuver when an accident is imminent due to inattention of the driver are just one example of such ADAS. While these systems are already implemented in modern cars, collision avoidance systems (CAS) that additionally conduct autonomous evasion maneuvers are part of ongoing research, see e.g. [1], [2].

In this context, RWTH Aachen University conducts research on a CAS that relies on a global navigation satellite system (GNSS) in combination with digital road maps and vehicle-to-vehicle (V2V) communication, see [2]. The intended behavior of CAS is to keep track of surrounding vehicles and to conduct an autonomous emergency braking resp. evasion maneuver if the driver does not react appropriately in time. This contribution focuses on the control approach to guide the vehicle on a desired evasion trajectory at the handling limits. As the evasion trajectory, provided by a trajectory planner, is considered to be given over a finite time horizon and physical constraints like the tire/road friction limit shall be taken into account, a model-based predictive control (MPC) scheme [3] is investigated.

"Galileo above" is funded by the Federal Ministry of Economics and Technology, in compliance with a resolution of the German Parliament.

A. Katriniok, J.P. Maschuw and D. Abel are with the Institute of Automatic Control, Department of Mechanical Engineering, RWTH Aachen University, 52074 Aachen, Germany, {A.Katriniok, J.Maschuw, D.Abel}@irt.rwth-aachen.de

F. Christen works at Forschungsgesellschaft Kraftfahrwesen mbH Aachen, 52074 Aachen, Germany, Christen@fka.de

L. Eckstein is with the Institute of Automotive Engineering, Department of Mechanical Engineering, RWTH Aachen University, 52074 Aachen, Germany, Eckstein@ika.rwth-aachen.de

B. Related Work and Main Contribution

Regarding MPC-based vehicle guidance, [4] introduces a nonlinear steering-only MPC controller (NMPC) for an obstacle avoidance as well as a side-wind rejection maneuver. For the same purpose, [5] introduces a hybrid parameter-varying MPC (HPV-MPC) which aims at reducing the computational complexity of [4]. A linear time-varying MPC (LTV-MPC) approach using successive linearizations of the nonlinear prediction model is investigated in [6]. While [6] limits the tire sideslip angles to the linear region, a LTV-MPC steering-only controller that is able to guide the vehicle at the handling limits, i.e. in the nonlinear region of the tire model, has been proposed by the authors in [7]. The additional use of differential braking can be found in [8].

Subsequently, the main focus is on the design of a MPC-based controller that employs the wheel steering angle and the vehicle's longitudinal acceleration (in contrast to differential braking in [8]) as control inputs to follow an evasion trajectory at the handling limits. As the underlying application aims at avoiding accidents, only negative accelerations are considered to be reasonable as positive accelerations might even worsen the consequences of a collision. A LTV-MPC control scheme has been chosen to cover model nonlinearities while being able to apply the controller in real-time during experimental tests. The main contribution of this paper can be seen in the formulation as multiple-input multiple-output (MIMO) trajectory following problem which is handled in the sense of an integrated vehicle dynamics control approach. In this regard, the trajectory following problem is decomposed in a path following problem, having the main objective to minimize the lateral deviation from the evasion path, and a velocity trajectory tracking problem. To the best knowledge of the authors, this particular control problem has not been investigated so far.

Consecutively, section II describes the employed prediction model that is used in the control scheme outlined in section III. Finally, experimental results are discussed in section IV.

978-3-033-03962-9/©2013 EUCA

II. MODELING

A. Vehicle Model and Relative Kinematics

In order to describe vehicle dynamics, a nonlinear single-track model according to [9] is employed, see Fig. 1. In this regard, it is assumed that the height of center of gravity (CG) is zero, thus neglecting roll and pitch dynamics, and that rolling resistances, aerodynamic drag as well as road bank and grade are negligible. Table I provides an overview of the employed model parameters. Particularly, Newton-Euler equations (1)-(2) denote the longitudinal and lateral momentum with respect to CG in the vehicle reference frame while yaw dynamics are considered by (3). Compared to the steering-only approach in [7], the longitudinal deceleration $a_{x,br}$ due to braking as well as the corresponding longitudinal tire forces $F_{x,f}$ and $F_{x,r}$ are additionally incorporated in (1)-(3). The particular computation of $F_{x,f}$ and $F_{x,r}$ in dependence of $a_{x,br}$ is introduced in section II-B.

$$\dot{v}_x = \dot{\psi} v_y - \frac{1}{m} F_{y,f} \sin(\delta) + a_{x,br} \tag{1}$$

$$\dot{v}_y = -\dot{\psi} v_x + \frac{1}{m}\Big(F_{y,f}\cos(\delta) + F_{y,r} + F_{x,f}\sin(\delta)\Big) \tag{2}$$

$$\ddot{\psi} = \frac{1}{J_z}\Big(F_{y,f}\cos(\delta) l_f + F_{x,f}\sin(\delta) l_f - F_{y,r} l_r\Big) \tag{3}$$

Furthermore, the dynamic behavior of the steering actuator is approximated by a first-order lag element

$$\dot{\delta} = -\frac{1}{T_\delta}\delta + \frac{1}{T_\delta}\delta_{ref} \tag{4}$$

where T_δ denotes the dynamic time constant, δ_{ref} the demanded and δ the actual wheel steering angle. Likewise, the dynamic behavior of the braking system is modeled by

$$\dot{a}_{x,br} = -\frac{1}{T_{a_{x,br}}} a_{x,br} + \frac{1}{T_{a_{x,br}}} a_{x,br,ref} \tag{5}$$

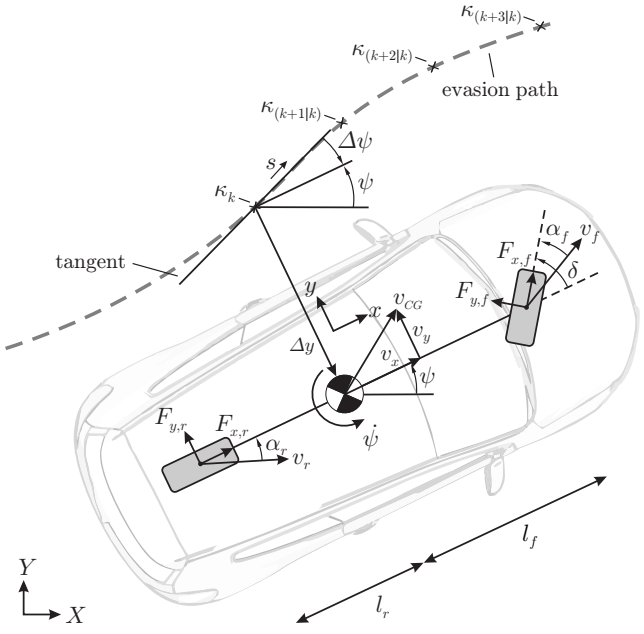

Fig. 1. Free body diagram of the employed prediction model

TABLE I
EMPLOYED SYMBOLS

Symbol	Description
m	Vehicle mass
J_z	Mass moment of inertia (vertical axis)
μ	Maximum tire/road friction coefficient
l_f, l_r	Distance between CG and front/rear axle
v_x, v_y	Longitudinal/lateral velocity at CG in veh. ref. frame
$\dot{\psi}$, ψ	Yaw rate, yaw angle
$\Delta\psi$	Difference angle between vehicle and evasion path
Δy	Lateral distance between CG and evasion path
$d_{\Delta\dot{y}}$	Lateral velocity disturbance
δ	Actual wheel steering angle at the front axle
δ_{ref}	Demanded wheel steering angle at the front axle
$a_{x,br}$	Actual deceleration due to braking
$a_{x,br,ref}$	Demanded deceleration due to braking
i_{br}	Brake force distribution front/rear axle
T_δ	Dynamic time constant of steering system
$T_{a_{x,br}}$	Dynamic time constant of braking system
κ	Path curvature
α_f, α_r	Sideslip angle at the front/rear tire
$F_{x,f}$, $F_{x,r}$	Applied longitudinal forces at the front/rear tire
$F_{y,f}$, $F_{y,r}$	Applied lateral forces at the front/rear tire
$F_{z,f}$, $F_{z,r}$	Vertical tire load at the front/rear tire
v_{CG}	Absolute velocity at CG
v_f, v_r	Absolute velocity at the front/rear tire

where $T_{a_{x,br}}$ indicates the dynamic time constant, $a_{x,br,ref}$ the demanded and $a_{x,br}$ actual longitudinal deceleration due to braking.

The relative rotational and translational movement between the vehicle's CG and the evasion path is described by (6)-(7) in accordance to [7]. In this context, $\Delta\psi$ denotes the relative yaw angle, Δy the lateral distance between the vehicle's CG and the evasion path perpendicular to the longitudinal vehicle axis and κ the path's curvature.

$$\Delta\dot{\psi} = \dot{\psi} - \kappa\sqrt{{v_x}^2 + {v_y}^2} \tag{6}$$

$$\Delta\dot{y} = \sqrt{{v_x}^2 + {v_y}^2}\sin(\Delta\psi) + v_y + d_{\Delta\dot{y}} \tag{7}$$

$$\dot{d}_{\Delta\dot{y}} = 0 \tag{8}$$

As described in [6], yaw angle offsets can be observed in experimental tests. Such a yaw angle offset can be interpreted as a lateral velocity disturbance acting on the relative lateral velocity $\Delta\dot{y}$ in (7) and thus as a ramp disturbance on Δy. To achieve steady-state offset-free tracking and to improve the transient tracking performance, the yaw angle offset is modeled as a lateral velocity disturbance $d_{\Delta\dot{y}}$. The corresponding dynamic behavior (8) is assumed to be a random walk-process. Further information on disturbance estimation is provided in section III-C.

B. Tire Model

1) Longitudinal Tire Forces: As outlined in section II-A, longitudinal tire forces $F_{x,f}$ and $F_{x,r}$ have to be determined in dependence of $a_{x,br}$. In this context, the longitudinal momentum due to braking can be expressed as

$$m \cdot a_{x,br} = F_{x,f}\cos(\delta) + F_{x,r}. \tag{9}$$

Defining the front/rear tire force distribution i_{br} as

$$i_{br} = \frac{F_{x,f}}{F_{x,f} + F_{x,r}}, \tag{10}$$

the corresponding longitudinal front resp. rear tire forces can be formulated as

$$F_{x,f} = \frac{i_{br}}{1 - i_{br}} F_{x,r}, \quad F_{x,r} = \frac{1 - i_{br}}{i_{br}} F_{x,f} \tag{11}$$

when reorganizing (10) with respect to $F_{x,f}$ resp. $F_{x,r}$. When substituting (11) in (9), $F_{x,f}$ resp. $F_{x,r}$ can be determined as a nonlinear function of $a_{x,br}$

$$F_{x,f} = \frac{m}{\cos(\delta) + \frac{1-i_{br}}{i_{br}}} \cdot a_{x,br}, \tag{12}$$

$$F_{x,r} = \frac{m}{1 + \frac{i_{br}}{1-i_{br}} \cos(\delta)} \cdot a_{x,br}. \tag{13}$$

For the sake of simplicity, it is asssumed that the ideal brake force distribution [10]

$$i_{br} = \frac{F_{z,f}}{F_{z,f} + F_{z,r}} = \frac{l_r}{l_f + l_r} \tag{14}$$

is applied by the braking system, where

$$F_{z,f} = \frac{m \cdot g \cdot l_r}{l_f + l_r}, \quad F_{z,r} = \frac{m \cdot g \cdot l_f}{l_f + l_r} \tag{15}$$

denotes the nominal tire load neglecting load transfer, see [9].

2) Lateral Tire Forces at Pure Cornering: To determine the lateral tire forces $F_{y,f}$ and $F_{y,r}$ in (1)-(3), a Pacejka Magic Formula tire model [11] is employed. When assuming pure cornering, the corresponding lateral tire forces $F_{y,i,0}$ for $i \in \{f, r\}$ can be expressed as

$$F_{y,i,0} = \mu F_{z,i} \cdot f_{y,i}(\alpha_i) \tag{16}$$

where $\mu F_{z,i}$ indicates the maximum feasible lateral tire force according to Coulomb's law of friction and $f_{y,i}(\alpha_i)$ the normalized Pacejka Magic Formula. In this regard, α_i denotes the tire sideslip angle at the front resp. the rear tire according to [7], μ the maximum friction coefficient and $F_{z,i}$ the nominal tire load as defined in (15).

3) Combined Slip: An extension of the Pacejka tire model that allows for considering combined slip, i.e. the simultaneous transmission of longitudinal and lateral forces, is proposed in [11]. Due to the fact that this concept requires additional parameters to be identified, a simplified approach according to [12] is employed in this contribution. In particular, the lateral tire force $F_{y,i,0}$ for $i \in \{f, r\}$ at pure cornering is reduced depending on the transmission of longitudinal forces in accordance to the friction ellipse

$$F_{y,i} = F_{y,i,0} \sqrt{1 - \left(\frac{F_{x,i}}{F_{x,i,max}} \right)^2} \tag{17}$$

where

$$F_{x,i,max} = \begin{cases} \mu F_{z,i} \ , & \|F_{x,i}\| < \mu F_{z,i} \\ \xi_{F_x} \|F_{x,i}\| \ , & \|F_{x,i}\| \geq \mu F_{z,i} \end{cases} \tag{18}$$

with $\xi_{F_x} > 1$ descibes the maximum feasible longitudinal tire force. As the maximum friction coefficient μ is not known exactly and load transfer is neglected, the longitudinal tire forces that are determined by (12)-(13) in dependence of $a_{x,br}$ can exceed the assumed friction limit $\mu F_{z,i}$. Furthermore, $F_{x,i}/F_{x,i,max} < 1$ has to be ensured to avoid linearization issues. Thus, the maximum feasible force $F_{x,i,max}$ is increased to a slightly larger value than the absolute value of the longitudinal tire force $F_{x,i}$ if $\|F_{x,i}\| \geq \mu F_{z,i}$. For this purpose, ξ_{F_x} is introduced in (18) and has to be chosen slightly larger than one.

C. Resulting Prediction Model

Finally, replacing $F_{x,i}$ resp. $F_{y,i}$ in (1)-(3) with (12)-(13) resp. (17) and using the lateral deviation Δy from the evasion path as well as the absolute velocity $v_{CG} = \sqrt{v_x^2 + v_y^2}$ at CG as control outputs, the resulting nonlinear prediction model can be rewritten in state space representation as

$$\dot{\boldsymbol{x}} = \boldsymbol{f}(\boldsymbol{x}, \boldsymbol{u}, z) \tag{19}$$

$$\boldsymbol{y} = \boldsymbol{g}(\boldsymbol{x}) = \begin{bmatrix} \Delta y \\ v_{CG} \end{bmatrix} \tag{20}$$

where $\boldsymbol{x}^T = [v_x, \ v_y, \ \dot{\psi}, \ \delta, \ a_{x,br}, \ \Delta\psi, \ \Delta y, \ d_{\Delta\dot{y}}]$ denotes the state vector, $\boldsymbol{u}^T = [\delta_{ref}, \ a_{x,br,ref}]$ the input vector and $z = \kappa$ the system disturbance. To be used in the predictive control approach, (19)-(20) have to be linearized at the current operating point $(\boldsymbol{x}_0, \boldsymbol{u}_0, z_0)$ and to be transfered into a discrete-time representation. Finally, the resulting discrete-time linear affine prediction model can be written as

$$\boldsymbol{x}_{k+1} = \boldsymbol{A}_k \boldsymbol{x}_k + \boldsymbol{B}_k \boldsymbol{u}_k + \boldsymbol{E}_k z_k + \boldsymbol{\Gamma}_k \tag{21}$$

$$\boldsymbol{y}_k = \boldsymbol{C}_k \boldsymbol{x}_k + \boldsymbol{\Pi}_k \tag{22}$$

where $\boldsymbol{A}_k \in \mathbb{R}^{8\times8}$ denotes the system matrix, $\boldsymbol{B}_k \in \mathbb{R}^{8\times2}$ the input matrix, $\boldsymbol{C}_k \in \mathbb{R}^{2\times8}$ the output matrix, $\boldsymbol{E}_k \in \mathbb{R}^8$ describes the influence of the system disturbance z on the state variables and $\boldsymbol{\Gamma}_k \in \mathbb{R}^8$ as well as $\boldsymbol{\Pi}_k \in \mathbb{R}^2$ indicate affine terms that result from the linearization of (19)-(20).

III. OPTIMAL VEHICLE DYNAMICS CONTROL

A. Problem Statement

As outlined in section I, the main aim of the controller is to follow an evasion trajectory by demanding the wheel steering angle δ_{ref} and the longitudinal deceleration $a_{x,br,ref}$. Thereby, the problem of trajectory following is decomposed in a path following problem, having the main objective to minimize the lateral deviation Δy from the evasion path, and a velocity trajectory tracking problem. As not all the states, required for this particular control approach, are directly measurable, two Extended Kalman Filter (EKF) [13] based estimators are employed to provide these states. The first, subsequently referred to as vehicle state estimator, determines the longitudinal velocity v_x, the lateral velocity v_y as well as the yaw rate $\dot{\psi}$. Based on the estimator outputs, the longitudinal acceleration due to braking $a_{x,br}$ is computed based on the measured acceleration $a_x = \dot{v}_x - \dot{\psi} v_y$ substracting the resistance $-\frac{1}{m} F_{y,f} \sin(\delta)$ due to steering,

see (1). As the vehicle state estimator is not part of this contribution, it is subsequently assumed to provide information with sufficient accuracy. The second estimator is employed for the purpose of disturbance estimation and supplies $\Delta\psi$, Δy and $d_{\Delta\dot{y}}$, see section III-C. Finally, the actual wheel steering angle δ is obtained from the vehicle.

B. Predictive Control Problem

In general, the main idea of MPC-based control schemes is to employ a mathematical plant model to predict the plant's outputs $\boldsymbol{y}_{(k+j|k)}$, $j = 1, .., H_p$ over a finite predicition horizon of length H_p. In this context, $\{\cdot\}_{(k+j|k)}$ indicates that at time k the future value of variable $\{\cdot\}$ is predicted for time $k + j$. According to this prediction, the control inputs are chosen in such a way over a finite control horizon of length H_u that the deviations from a reference trajectory $\boldsymbol{r}_{(k+j|k)}$, $j = 1, ..., H_p$ are minimized according to a quadratic cost function. This open-loop control problem is solved at each sampling time, thus obtaining an optimal input step sequence $\boldsymbol{\Delta u}^*_{(k|k)}, ..., \boldsymbol{\Delta u}^*_{(k+H_u-1|k)}$. Finally, the control input $\boldsymbol{u}_k = \boldsymbol{u}_{k-1} + \boldsymbol{\Delta u}^*_{(k|k)}$ is applied to the plant where $\boldsymbol{u}_{k-1}$ denotes the control input of the preceding time step $k-1$. At the next time step, this optimization is repeated over a shifted prediction horizon.

As far as this particular control problem is concerned, the control outputs comprise the lateral deviation Δy from the evasion path as well as the absolute velocity v_{CG} at CG. While the reference value of the lateral deviation $r_{\Delta y,(k+j|k)}$ is set to zero, the velocity reference value $r_{v_{CG},(k+j|k)}$ is provided by the trajectory planner. Due to the fact that the predicition model is inherently nonlinear, especially when operating at the vehicle handling limits, successive linearizations of the nonlinear plant model (19)-(20) are determined at the operating point $(\boldsymbol{x}_0 = \boldsymbol{x}_k,\ \boldsymbol{u}_0 = \boldsymbol{u}_{k-1},\ z_0 = \kappa_k)$ in each sampling step at time k, thus obtaining a LTV-MPC control scheme. In this regard, $\boldsymbol{x}_k$ indicates the state vector at time k, $\boldsymbol{u}_{k-1}$ the control input of the preceding time step $k-1$ and κ_k the path's curvature at time k. The resulting discrete-time linear affine plant model (21)-(22) is employed to determine the free response of the plant and to formulate the constrainted finite-time optimal control problem (CFTOC). When predicting the free response of the plant, the path's curvature κ_k at time k results from the perpendicular projection of the vehicle's CG on the evasion path, see Fig. 1. For the remaining prediction horizon, $\kappa_{(k+j|k)}$, $j = 1, ..., H_p - 1$ is estimated assuming that the vehicle follows the evasion path in an optimal way along the path coordinate s. Using the quadratic cost function

$$J(\boldsymbol{\Delta u}, \epsilon_f, \epsilon_r) = \sum_{j=1}^{H_p-1} \boldsymbol{e}^T_{(k+j|k)} \boldsymbol{Q} \boldsymbol{e}_{(k+j|k)} \tag{23a}$$

$$+ \boldsymbol{e}^T_{(k+H_p|k)} \boldsymbol{Q}_{H_p} \boldsymbol{e}_{(k+H_p|k)} \tag{23b}$$

$$+ \sum_{j=0}^{H_u-1} \boldsymbol{\Delta u}^T_{(k+j|k)} \boldsymbol{R} \boldsymbol{\Delta u}_{(k+j|k)} \tag{23c}$$

$$+ \rho_f \cdot \epsilon_f + \rho_r \cdot \epsilon_r \tag{23d}$$

with $\boldsymbol{e}_{(k+j|k)} = \boldsymbol{y}_{(k+j|k)} - \boldsymbol{r}_{(k+j|k)}$, the CFTOC of the trajectory following problem can be formulated as

$$\min_{\boldsymbol{\Delta u}, \epsilon_f, \epsilon_r} J(\boldsymbol{\Delta u}, \epsilon_f, \epsilon_r) \tag{24a}$$

subject to

dynamic constraints

$$\boldsymbol{x}_{k+1} = \boldsymbol{A}_k \boldsymbol{x}_k + \boldsymbol{B}_k \boldsymbol{u}_k + \boldsymbol{E}_k z_k + \boldsymbol{\Gamma}_k \tag{24b}$$

$$\boldsymbol{y}_k = \boldsymbol{C}_k \boldsymbol{x}_k + \boldsymbol{\Pi}_k \tag{24c}$$

input constraints

$$\boldsymbol{\Delta u}_{(k+j|k)} \geq \boldsymbol{\Delta u}_{min}, \qquad j = 0, ..., H_u - 1 \tag{24d}$$

$$\boldsymbol{\Delta u}_{(k+j|k)} \leq \boldsymbol{\Delta u}_{max}, \qquad j = 0, ..., H_u - 1 \tag{24e}$$

$$\boldsymbol{u}_{(k+j|k)} \geq \boldsymbol{u}_{min}, \qquad j = 0, ..., H_u - 1 \tag{24f}$$

$$\boldsymbol{u}_{(k+j|k)} \leq \boldsymbol{u}_{max}, \qquad j = 0, ..., H_u - 1 \tag{24g}$$

and state constraints

$$\alpha_{f,(k+j|k)} \geq \alpha_{f,min} - \epsilon_f, \qquad j = 1, ..., H_p \tag{24h}$$

$$\alpha_{f,(k+j|k)} \leq \alpha_{f,max} + \epsilon_f, \qquad j = 1, ..., H_p \tag{24i}$$

$$\alpha_{r,(k+j|k)} \geq \alpha_{r,min} - \epsilon_r, \qquad j = 1, ..., H_p \tag{24j}$$

$$\alpha_{r,(k+j|k)} \leq \alpha_{r,max} + \epsilon_r, \qquad j = 1, ..., H_p \tag{24k}$$

$$\epsilon_f \geq 0,\ \epsilon_r \geq 0 \tag{24l}$$

where $\boldsymbol{\Delta u}^T = [\boldsymbol{\Delta u}^T_{(k|k)}, ..., \boldsymbol{\Delta u}^T_{(k+H_u-1|k)}]$. As far as the quadratic cost function (23) is concerned, (23a)-(23b) weigh the deviation of the control outputs from their reference values, (23c) the shift per time step of the control inputs and (23d) the use of the slack variables ϵ_f resp. ϵ_r that are employed in soft constraints (24h)-(24k). To apply the control scheme online and in real-time, the control horizon H_u is always chosen shorter than the prediction horizon H_p to reduce computation time. In this regard, investigations have shown that using terminal cost (23b), i.e. a significantly increased weight at the end of the prediction horizon, leads to a noticeable improvement of the control performance. Thereby, it has to be noted that the control scheme is stable without any appropriately chosen terminal cost. Indeed, the main intention of employing (23b) is to force the control outputs to tend towards their reference values at the end of the prediction horizon which has turned out to be beneficial.

Input constraints (24d)-(24g) are introduced to account for limitations of the steering as well as the braking system. In particular, (24f)-(24g) are employed to limit the absoulte values of the control inputs while (24d)-(24e) constrain the corresponding maximum resp. minimum shift per time step. According to [6] and [7], soft constraints (24h)-(24k) on the tire sideslip angles have to be incorporated in the CFTOC to ensure vehicle stability when operating in the nonlinear region of the tire model. Due to the fact that the tire sideslip angles are a nonlinear function of the state variables, α_f and α_r are linearized at the current operating point at time k to obtain linear constraints and thus a convex optimization problem. The particular choise of the upper and lower tire sideslip angle limits is essential to ensure vehicle stability in the nonlinear region of the tire model. A detailed

discussion of this issue can be found in [7]. To ensure feasibility of the CFTOC (24), slack variables ϵ_f and ϵ_r are introduced to formulate state constraints (24h)-(24k). Finally, $\boldsymbol{Q} = diag(Q_{\Delta y}, Q_{v_{CG}})$, $\boldsymbol{Q}_{H_p} = diag(Q_{\Delta y,H_p}, Q_{v_{CG},H_p})$, $\boldsymbol{R} = diag(R_{\delta_{ref}}, R_{a_{x,br,ref}})$, ρ_f and ρ_r in (23) denote weighting matrices resp. coefficients.

C. Disturbance Estimation

As indicated in section II-A, time-varying yaw angle offsets can be observed in experimental tests, see [6]. These offsets can be interpreted as a lateral velocity disturbance with respect to the evasion path. Hence, yaw angle offsets act as a ramp disturbance on the control output Δy. To achieve offset-free tracking in MPC-based control schemes, an appropriate disturbance estimator is required if the plant itself does not contain enough integrators, see [14]. Thus, an EKF has been implemented to compensate the ramp disturbance on Δy in order to achieve steady-state offset-free tracking as well as to improve the transient control performance. For the second control output, i.e. the velocity v_{CG} at CG, disturbance estimation is not reasonable as the velocity can just be decreased by braking but not increased by accelerating. The EKF employs (6)-(8) as estimator model, thus obtaining the nonlinear estimation model

$$\dot{\boldsymbol{x}} = \boldsymbol{f}(\boldsymbol{x}, \boldsymbol{u}) \tag{25}$$

$$\boldsymbol{y} = [\Delta\psi,\ \Delta y]^T \tag{26}$$

where $\boldsymbol{x}^T = [\Delta\psi,\ \Delta y,\ d_{\Delta\dot{y}}]$ denotes the state vector, $\boldsymbol{u}^T = [v_x,\ v_y,\ \dot{\psi},\ \kappa]$ the input vector and $\boldsymbol{y}$ the measurement vector. In this context, κ and the measurement vector $\boldsymbol{y}$ are provided by the trajectory planner while the remaining inputs v_x, v_y and $\dot{\psi}$ are supplied by the vehicle state estimator. As an extension of [6], experimental results in section IV show that steady-state offsets of Δy can be avoided.

IV. EXPERIMENTAL RESULTS

A. Experimental Setup

For experimental tests, a Volkswagen Passat CC 3.6 V6 is employed as test vehicle. It is equipped with an electronic power steering (EPS) system which allows for demanding a wheel steering angle and a brake booster with a deceleration interface. Moreover, an Oxford RT3003 L1/L2 RTK-GPS/INS high precision navigation system (differential corrections are obtained via N-TRIP V3) provides the navigation solution, i.e. the vehicle's position, velocity and orientation, with an update rate of $100\,\mathrm{Hz}$. To handle the computational complexity of the applied algorithms, two dSPACE MicroAutoBox II electronic control units (ECU) are employed. In particular, sensor fusion algorithms (e.g. the vehicle state estimator) are assigned on the first while the control scheme is implemented on the second ECU. Thereby, the vehicle state estimator is executed with a sample time of $0.01\,\mathrm{s}$, the disturbance estimator with $0.02\,\mathrm{s}$ and the control scheme with $0.04\,\mathrm{s}$. Furthermore, qpOASES [15] is used as (active-set) QP solver while a solution of the CFTOC can always be obtained within the sampling interval resp. within the maximum number of iterations.

Consecutively, a scenario on a rural road with two lanes, oncoming traffic and a speed limit of $70\,\mathrm{km/h}$ is examined. The ego-vehicle is driving on a dry road ($\mu = 1$) with an initial velocity of $v_{CG} = 20\,\mathrm{m/s}$ when a non-moving broken vehicle occurs in the lane. At the same time, oncoming traffic on the other lane and a vehicle that is standing still on the same lane for a left turn ($50\,\mathrm{m}$ behind the first obstacle) are part of the scenario. For the evasion maneuver, the ego-vehicle has to evade the first obstacle as well as the oncoming traffic and has to decelerate to standstill before colliding with the turning vehicle. In order to be able to evade the oncoming traffic and to follow the evasion path, the inital velocity is decreased by braking with $-5\,\mathrm{m/s^2}$ from $t = 0$ to $0.8\,\mathrm{s}$ and with $-1.5\,\mathrm{m/s^2}$ from $t = 0.8$ to $1.3\,\mathrm{s}$ when lateral accelerations increase. In this time interval, braking and steering are applied simultaneously to investigate the potential of the proposed integrated vehicle dynamics control approach. From $t = 1.3$ to $3\,\mathrm{s}$, no further braking is applied to finish the main part of the maneuver as soon as possible. Finally, the vehicle is decelerated to standstill while braking is initiated with $-2\,\mathrm{m/s^2}$ from $t = 3$ to $5\,\mathrm{s}$ when the vehicle approaches its original lane. For $t > 5\,\mathrm{s}$, the velocity is reduced to zero by braking with $-8\,\mathrm{m/s^2}$. The corresponding reference path and velocity trajectory are depicted in Fig. 2. Thereby, the following MPC parameters have been used: $H_u = 15$, $H_p = 25$, $Q_{\Delta y} = 1$, $Q_{\Delta y,H_p} = 10$, $Q_{v_{CG}} = 0.15$, $Q_{v_{CG},H_p} = 1.5$, $R_{\delta_{ref}} = 200$, $R_{a_{x,br,ref}} = 1$, $\rho_f = 1000$, $\rho_r = 1000$, $\Delta\delta_{ref,max/min} = \pm 0.8\,\mathrm{deg}$, $\delta_{ref,max/min} = \pm 15\,\mathrm{deg}$, $\Delta a_{x,br,max/min} = \pm 9.81\,\mathrm{m/s^2}$, $a_{x,br,ref,max} = 0\,\mathrm{m/s^2}$, $a_{x,br,ref,min} = -9.81\,\mathrm{m/s^2}$.

B. Evaluation of Experimental Results

Fig. 2 depicts the results that have been gained in experimental tests. As far as the control outputs are concerned, a maximum lateral deviation error $e_{\Delta y,max}$ of $0.25\,\mathrm{m}$ resp. a root mean square error (RMSE) $e_{\Delta y,RMSE}$ of $0.12\,\mathrm{m}$ can be observed. The absolute velocity v_{CG} at CG shows a maximum tracking error $e_{v_{CG},max}$ of $1.55\,\mathrm{m/s}$ resp. a RMSE $e_{v_{CG},RMSE}$ of $0.99\,\mathrm{m/s}$. These velocity errors as well as the delayed response of v_{CG} from $t = 0$ to $0.3\,\mathrm{s}$ are mainly caused by the inital buildup of the brake booster pressure and cannot be avoided. As the controller is not able to accelerate, the velocity decreases from $t = 1.3$ to $3.4\,\mathrm{s}$ due to steering and rolling resistances. For $t \geq 3.4\,\mathrm{s}$ the velocity is tracked very well. Though, it can be recognized that the maneuver ends at a velocity of about $2\,\mathrm{m/s}$ instead of standstill. This issue is caused by the fact that the estimators as well as the controller are disabled for low velocities to avoid numerical issues. During the maneuver, horizontal accelerations increase up to $8.9\,\mathrm{m/s^2}$ when steering and braking is applied simultaneously which corresponds to the limits of vehicle dynamics. Thereby, longitudinal accelerations have a magnitude of $-9.3\,\mathrm{m/s^2}$ while lateral accelerations are in a range of $\pm 6.7\,\mathrm{m/s^2}$. Considering tire sideslip angles, it is apparent that the maximum absolute tire sideslip angle at the front axle amounts to $4.7\,\mathrm{deg}$ while the limit of static friction

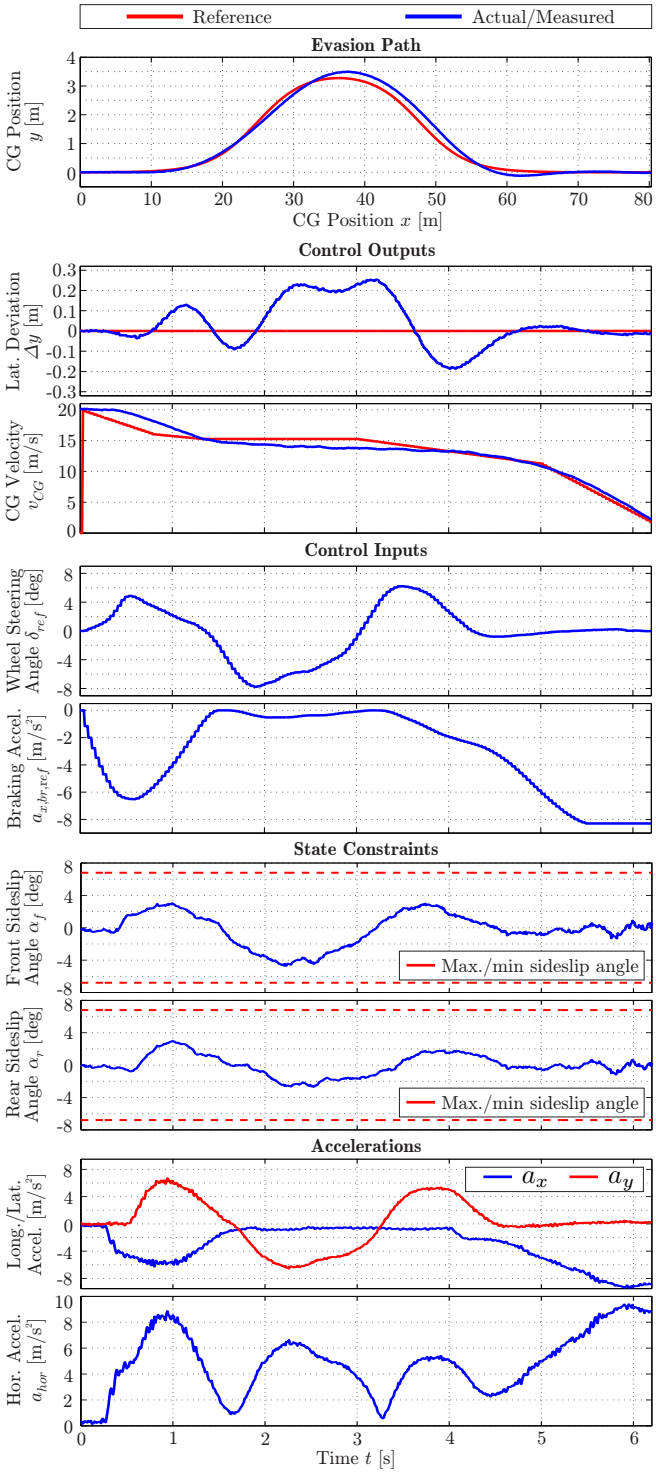

Fig. 2. Experimental results

corresponds to 7 deg. Thereby, it has to be stated that linear tire behavior can be assumed for $-3\,\text{deg} \geq \alpha_i \geq 3\,\text{deg}$ and that 95% of the maximum feasible tire force is transmitted for sideslip angles of $\pm 5\,\text{deg}$. According to the main focus of this paper, it can be concluded that the controller is able to guide the vehicle at the handling limits when combined steering and braking is applied (especially for $t = 0.5$ to 1.5 s) as well as in the nonlinear region of the (lateral) tire force model (especially for $t = 1.8$ to 2.8 s) while achieving a convincing control performance. Finally, steady-state offsets of the lateral deviation Δy can be avoided using the disturbance estimator outlined in section III-C.

V. CONCLUSION AND FUTURE WORK

In this paper, an optimal control approach for combined longitudinal and lateral vehicle guidance at the handling limits is introduced. The control problem to follow an evasion trajectory is decomposed in a path following and a velocity trajectory tracking problem. Thereby, the controller inherently considers the combined transmission of longitudinal and lateral forces in the sense of an integrated vehicle dynamics control approach. Experimental results prove the potential of the proposed control scheme.

As far as future work is concerned, the incorporation of load transfer due to braking into the prediction model will be investigated. As braking leads to a higher/lower tire load at the front/rear axle, a larger/smaller amount of tire forces can be transmitted at this axle. Hence, it has to be proven if an improved control performace can be achieved when this information is considered in the prediction model.

REFERENCES

[1] R. Isermann, R. Mannale, and K. Schmitt, "Collision-avoidance systems PRORETA: Situation analysis and intervention control," *Control Engineering Practice*, vol. 20, no. 11, pp. 1236–1246, 2012.

[2] A. Katriniok, M. Reiter, D. Abel, F. Christen, and L. Eckstein, "Collision Avoidance using Galileo - The automotiveGATE as Development and Testing Center for Galileo based Applications," in *Aachener Colloquium Automobile and Engine Technology*, 2010.

[3] J. Maciejowski, *Predictive Control with Constraints*. Prentice Hall, Harlow, 2002.

[4] T. Keviczky, P. Falcone, F. Borrelli, J. Asgari, and D. Hrovat, "Predictive control approach to autonomous vehicle steering," in *American Control Conference*, 2006, pp. 4670–4675.

[5] T. Besselmann and M. Morari, "Hybrid Parameter-varying Model Predictive Control for Autonomous Vehicle Steering," *European Journal of Control*, vol. 14, no. 5, pp. 418–431, 2008.

[6] P. Falcone, F. Borrelli, J. Asgari, H. E. Tseng, and D. Hrovat, "Predictive Active Steering Control for Autonomous Vehicle Systems," *IEEE Transactions on Control Systems Technology*, vol. 15, no. 3, pp. 566–580, 2007.

[7] A. Katriniok and D. Abel, "LTV-MPC Approach for Lateral Vehicle Guidance by Front Steering at the Limits of Vehicle Dynamics," in *IEEE Conference of Decision and Control and European Control Conference*, 2011, pp. 6828–6833.

[8] P. Falcone, F. Borrelli, J. Asgari, H. Tseng, and D. Hrovat, "A model predictive control approach for combined braking and steering in autonomous vehicles," in *Mediterranean Conference on Control Automation*, 2007, pp. 1–6.

[9] R. Rajamani, *Vehicle Dynamics and Control*. Springer, 2006.

[10] M. Mitschke and H. Wallentowitz, *Dynamik der Kraftfahrzeuge*. Springer Verlag, 2004.

[11] H. Pacejka and E. Bakker, "The magic formular tire model," *Vehicle System Dynamics: International Journal of Vehicle Mechanics and Mobility*, vol. 21, no. 1, pp. 1–18, 1992.

[12] B. Johansson and M. Gäfvert, "Untripped SUV Rollover Detection and Prevention," in *IEEE Conference on Decision and Control*, 2004, pp. 5461–5466.

[13] D. Simon, *Optimal State Estimation: Kalman, H Infinity, and Nonlinear Approaches*. John Wiley & Sons, Inc., 2006.

[14] M. Morari and U. Maeder, "Nonlinear offset-free model predictive control," *Automatica*, vol. 48, no. 9, pp. 2059 – 2067, 2012.

[15] H. J. Ferreau, "qpOASES User's Manual (Version 3.0beta)," *Optimization in Engineering Center (OPTEC) and Department of Electrical Engineering, KU Leuven*, 2012.